Orient Academies

Real-Time Mechanistic Anomaly Detection in Drilling: Bayesian Fusion of Reduced-Order Multiphase Flow and Surface Data

Adel Benamar[1], Karim Selmani[2]

Abstract

Drilling operations routinely rely on surface instrumentation to infer evolving downhole conditions, yet the mapping from surface signals to annular multiphase states remains underdetermined when flow transitions and sensor artifacts co-occur. In managed-pressure and deepwater contexts, early recognition of anomalous influx signatures is particularly challenging because small deviations in pressure, flow, and pump behavior can be consistent with multiple latent mechanisms. This paper develops a physics-constrained digital-twin framework that fuses reduced-order multiphase flow dynamics with uncertainty-aware representation learning to detect, localize, and quantify anomalies in real time using primarily surface measurements. The central contribution is a differentiable observer that embeds a quasi-one-dimensional annular flow model inside a probabilistic state-space estimator while learning only the closure discrepancies needed to reconcile model and data. Unlike purely discriminative detectors, the proposed approach outputs calibrated posterior distributions over latent annular states, regime-consistent transport parameters, and an anomaly score tied to mechanistic residuals. The method supports both abrupt events and slowly drifting conditions through Bayesian change detection on innovation statistics, and it provides decision support by mapping posterior risk to constraint-aware operational advisories. The paper details identifiability conditions, stabilization via dissipativity constraints, and robustification to sensor delays and rate limits. A comprehensive evaluation protocol is proposed to quantify detection latency, false-alarm control, and out-of-distribution generalization across geometries and fluids without assuming access to downhole labels.

[1] Université d'El Tarf, Avenue Colonel Amirouche 27, El Tarf 36000, Algeria
[2] Université de Naâma„ Route Sidi Ahmed 19, Naâma 45000, Algeria

Contents

1. Introduction

Surface sensing is attractive in drilling because it is ubiquitous, accessible, and comparatively reliable, but it is also intrinsically indirect [1]. Pressure, flow, and pump measurements represent a compressed projection of a distributed multiphase transport process occurring along a long, tortuous wellbore with evolving boundary conditions. The operational objective is not merely to classify a measurement window as normal or abnormal, but to infer what physical state could plausibly generate the observation while quantifying uncertainty that arises from model error, unknown fluid properties, and unmeasured disturbances. The difficulty is intensified by regime transitions in gas–liquid mixtures, where slip, compressibility, and friction closure choices can change abruptly, and where the same surface pressure deviation can be explained by competing latent causes such as cuttings

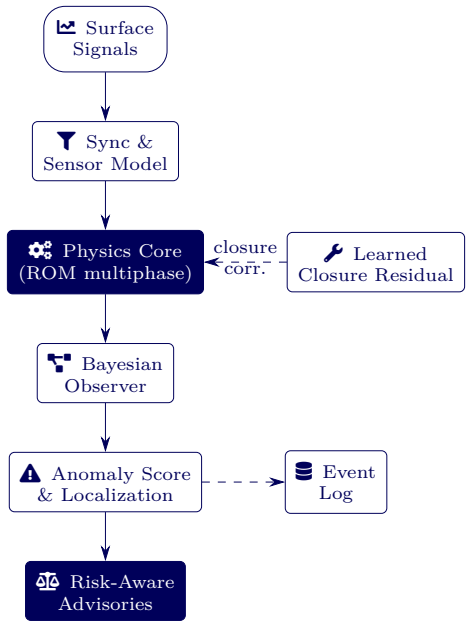

Figure 1. End-to-end digital-twin workflow: synchronized surface measurements drive a reduced-order multiphase physics core augmented by bounded closure corrections; a Bayesian observer maintains posteriors over latent annular states and residual channels, producing probabilistic anomaly evidence that is mapped to risk-aware advisories and logged for audit and calibration.

loading, rheology drift, choke movement, or a developing influx [2]. In this setting, a detector that produces a binary label without a calibrated confidence and without a mechanistic diagnosis is operationally brittle: it can alarm too late when confronted with atypical transients, or it can over-alarm in the presence of benign disturbances, eroding trust and encouraging alarm suppression.

Recent machine-learning approaches have shown that surface-accessible signals can contain useful information for kick symptom identification, with high predictive accuracy under controlled conditions and engineered features [3]. While such results help establish feasibility, a practical real-time system must address three additional requirements that are often peripheral in purely predictive studies. First, it must remain stable and interpretable when the well geometry, fluid properties, and operational envelope differ from those seen in training [4]. Second, it must quantify uncertainty rather than only providing point predictions, because operational decisions are constrained by safety margins and the cost of false positives can be substantial. Third, it must represent dynamics: influx growth, gas migration, compressibility, and choke-pump interactions unfold over time and cannot be faithfully captured by static snapshots unless the detector implicitly learns a surrogate for the physics.

This paper argues that these requirements are best met by a hybrid approach: an explicitly mechanistic model supplies structure, conservation laws, and the correct inductive bias for extrapolation, while data-driven components account for closure mismatch, sensor idiosyncrasies, and unmodeled dynamics [5]. The central thesis is that a digital twin for wellbore anomaly detection should be formulated as a probabilistic observer for a constrained dynamical system, not as a standalone classifier. The technical contribution is a differentiable, uncertainty-aware observer that couples a reduced-order annular multiphase model to a learned closure module and performs online Bayesian state estimation from surface measurements. The observer is designed to be identifiable under realistic sensing limitations, to remain stable by construction through dissipativity and boundedness constraints, and to emit calibrated posteriors that can be mapped to risk-aware advisories.

The remainder of the paper proceeds by first defining a reduced-order, regime-consistent annular model suitable for embedding in real-time inference, then constructing a physics-constrained representation learning module that learns only what must be learned [6]. An online inference layer is developed to compute posteriors and detect change points with controlled false-alarm rates. Finally, a decision-support mapping is described, followed by an evaluation framework that emphasizes out-of-distribution robustness, detection latency, and calibration rather than only accuracy. Throughout, the goal is not to replace operational heuristics but to supply a mathematically grounded layer that translates surface evidence into probabilistic statements about downhole physical states and anomaly likelihood [7].

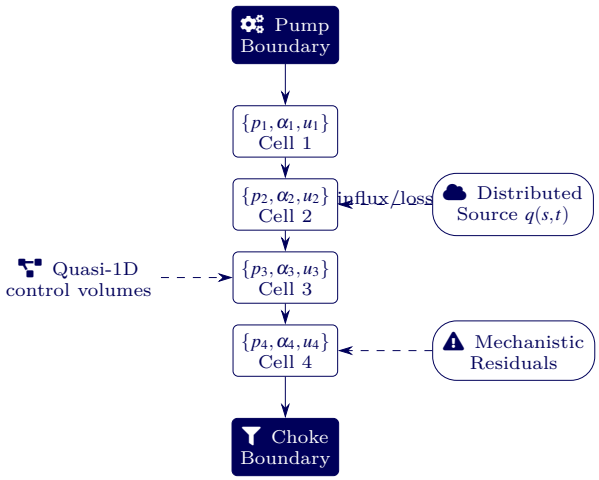

Figure 2. Reduced-order annular multiphase discretization: the wellbore is partitioned into control volumes with latent pressure, void fraction, and mixture velocity states, driven by pump/choke boundary conditions and reconciled with data via inferred distributed source terms and structured residual channels.

2. System Model

A digital twin intended for real-time anomaly detection must balance fidelity with computational tractability. Full two-fluid models with detailed closure can be too stiff for online inference when embedded in a Bayesian estimator, especially when parameter uncertainty is included. Conversely, overly simplified models risk confounding multiple mechanisms into an undifferentiated residual that is difficult to interpret. This section defines a reduced-order annular transport model that preserves the dominant couplings relevant to surface pressure signatures while supporting regime-consistent parameterization [8].

Consider a wellbore segment parameterized by measured depth coordinate $s \in [0, L]$ and time $t \geq 0$, with annular cross-sectional area $A_a(s)$ and hydraulic diameter $D_h(s)$. Let the mixture consist of a liquid phase (including drilling fluid and entrained solids treated as an effective liquid) and a gas phase. Define gas void fraction $\alpha(s,t)$, mixture density $\rho_m(s,t) = \alpha\rho_g(p,T) + (1-\alpha)\rho_\ell$, mixture velocity $u_m(s,t)$, and mixture pressure $p(s,t)$ [9]. A reduced drift-flux form captures slip through a closure for the gas velocity relative to the mixture. Let $u_g = C_0 u_m + V_{gj}$ denote the drift-flux relation, where C_0 is a distribution parameter and V_{gj} is a drift velocity that depends on regime, inclination, and local properties.

A quasi-one-dimensional conservation structure can be written as

$$\begin{aligned}
\frac{\partial}{\partial t}\left(\rho_m A_a\right) + \frac{\partial}{\partial s}\left(\rho_m u_m A_a\right) &= q_m(s,t), \\
\frac{\partial}{\partial t}\left(\alpha\rho_g A_a\right) + \frac{\partial}{\partial s}\left(\alpha\rho_g u_g A_a\right) &= q_g(s,t), \\
[10]\ \frac{\partial}{\partial t}\left(\rho_m u_m A_a\right) + \frac{\partial}{\partial s}\left(\rho_m u_m^2 A_a + p A_a\right) &= -A_a\rho_m g\sin\theta(s) \\
&\quad - \tau_w(s,t)P_w(s) + q_u(s,t).
\end{aligned} \tag{1}$$

where q_m represents distributed sources such as formation influx or loss, q_g is the gas source term, $\theta(s)$ is inclination, $P_w(s)$ is wetted perimeter, and τ_w is wall shear stress [11]. For real-time usage, the model is discretized into N control volumes yielding a finite-dimensional state vector. Let $x(t)$ collect cell-averaged quantities such as pressure, mixture velocity, and gas mass fraction, with dynamics

$$\dot{x}(t) = f\big(x(t), u(t), \vartheta(t)\big) + w(t), \tag{2}$$

where $u(t)$ denotes controlled boundary inputs such as pump rate and choke opening (or equivalent boundary pressure), $\vartheta(t)$ denotes slowly varying parameters including effective friction and slip coefficients, and $w(t)$ aggregates model discrepancy and process noise.

The measurement model reflects what surface sensors provide [12]. Let $y(t)$ include standpipe pressure, casing pressure, surface flow-in and flow-out, and pit volume rate when available. A key modeling choice is to explicitly represent sensor dynamics and delays, since rate-limited or filtered measurements can produce artifacts that mimic physical transients. The measurement model is [13]

$$y(t) = h\big(x(t), u(t)\big) + v(t), \tag{3}$$

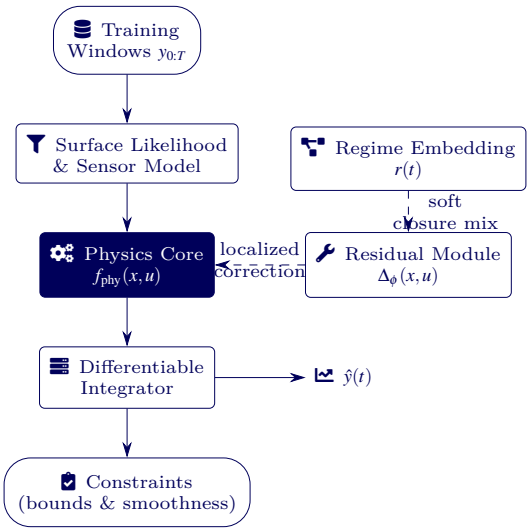

Figure 3. Hybrid learning decomposition: a conservation-structured physics core is augmented by a bounded residual module and a continuous regime embedding that interpolates closure families; end-to-end differentiability supports likelihood-based fitting on surface signals while enforcing physical constraints (e.g., bounded void fraction and stable closure corrections).

with $v(t)$ as measurement noise. When only a subset of surface signals is available, the mapping from x to y becomes highly non-injective, motivating the probabilistic formulation and the inclusion of structural priors.

To maintain regime consistency without enumerating regimes as discrete labels, this paper uses a continuous regime embedding $r(s,t)$ that interpolates between closure families [14]. The embedding influences drift-flux parameters, friction factors, and compressibility corrections. The embedding is not treated as a manually assigned label but as a latent variable inferred from data through regularized dynamics. The motivation is that flow-regime identification from two-phase data can be accurate when the feature space is expressive and the training set covers the operational envelope, as shown by high-performing neighborhood-based classifiers in vertical configurations [15], yet in real drilling the regime boundaries are uncertain and can shift with geometry and fluid changes [16]. A continuous embedding reduces brittleness by allowing soft transitions while still constraining closures to physically plausible manifolds.

The model must also incorporate boundary conditions that are consistent with drilling hydraulics. At the pump, flow-in sets an inlet mixture mass flux. At the choke, an outlet relation couples annular pressure to choke opening and downstream backpressure [17]. These relations can be captured by algebraic constraints appended to the state dynamics, producing a differential-algebraic form that is still amenable to differentiable simulation if the constraints are stabilized. The outcome of this section is a tractable, structured dynamical system that can generate surface observations from latent annular states, but with acknowledged mismatch due to uncertain closures and unmodeled effects. The next section explains how that mismatch is handled without surrendering physical interpretability [18].

3. Learning Architecture

A central design goal is to learn only what cannot be reliably specified from first principles while enforcing invariants that should hold across wells. The architecture therefore separates the model into a physics core and a learned closure residual. The physics core implements the discretized conservation dynamics and boundary relations. The learned component corrects selected closures such as wall shear and slip velocity, and it provides a compact representation of regime embedding dynamics [19]. This section formalizes that decomposition and the constraints used to ensure stable and physically plausible behavior.

Let the discretized physics core be written as $f_{\text{phy}}(x,u,\vartheta)$, where ϑ includes nominal closures. Introduce a learned residual $\Delta_\phi(x,u)$ with parameters ϕ, yielding

$$\dot{x}(t) = f_{\text{phy}}\big(x(t),u(t),\vartheta_0\big) + B\Delta_\phi\big(x(t),u(t)\big) + w(t). \tag{4}$$

The matrix B selects which state channels are modified by the learned residual to avoid unconstrained interference with conserved quantities [20]. For example, the residual may alter the shear stress term and drift-flux closure but not directly inject or remove mass. Concretely, the friction term can be expressed as

$$\tau_w(s,t) = \tau_{w,0}(x,u) + \Delta_{\phi,\tau}(x,u), \tag{5}$$

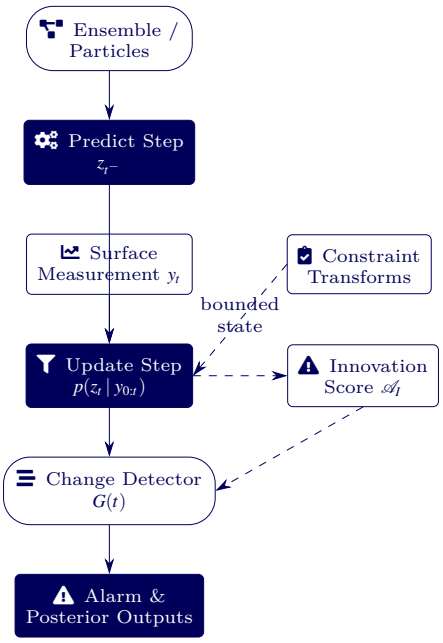

Figure 4. Online Bayesian inference loop: predictive propagation through the differentiable physics model is corrected by surface measurements under constraint-preserving transforms; innovation statistics and a sliding-window change detector convert posterior-consistent residual evidence into anomaly alarms and localized probabilistic diagnostics.

and slip parameters can be adjusted via

$$C_0(s,t) = \sigma\Big(C_{0,0}(x,u) + \Delta_{\phi,C}(x,u)\Big),$$
$$V_{gj}(s,t) = \mathrm{softplus}\Big(V_{gj,0}(x,u) + \Delta_{\phi,V}(x,u)\Big). \tag{6}$$

where $\sigma(\cdot)$ and $\mathrm{softplus}(\cdot)$ enforce boundedness and nonnegativity constraints implied by the closure definitions. These simple nonlinearities provide a hard barrier against physically impossible values without requiring post-hoc clipping that can break differentiability [21].

Because regime changes are a major source of nonlinearity, the architecture introduces a latent regime embedding $r(t)$ that evolves smoothly but can respond rapidly when evidence supports a transition. The embedding influences closure selection through a convex combination of K basis closures:

$$\tau_{w,0}(x,u,r) = \sum_{k=1}^{K} \pi_k(r)\, \tau_w^{(k)}(x,u),$$
$$V_{gj,0}(x,u,r) = \sum_{k=1}^{K} \pi_k(r)\, V_{gj}^{(k)}(x,u). \tag{7}$$

where $\pi_k(r)$ are nonnegative weights summing to one. Rather than treating r as a supervised label, it is inferred as part of the state, with dynamics [22]

$$\dot{r}(t) = g_\phi\big(r(t), x(t), u(t)\big) + \eta(t), \tag{8}$$

where g_ϕ is a learned function constrained to be contractive in r for stability, and $\eta(t)$ is a small diffusion term to prevent degeneracy in probabilistic inference.

Training such a hybrid model must contend with partial observability: downhole labels for $x(t)$ are rarely available. The architecture therefore uses self-supervised objectives defined on surface signals [23]. Let $\hat{y}(t)$ be the predicted surface measurements from the simulated state $\hat{x}(t)$. A basic objective is the negative log-likelihood under assumed measurement noise, but naive fitting can encourage the learned residual to absorb sensor noise or boundary artifacts. To prevent this, the learning objective is augmented with structural regularizers. A representative continuous-time form is

$$\mathscr{L}(\phi) = \int_0^T \Big(\big(y(t) - \hat{y}(t)\big)^\top R^{-1} \big(y(t) - \hat{y}(t)\big) + \lambda_\Delta \|\Delta_\phi(\hat{x}(t), u(t))\|^2 + \lambda_E\, \Psi\big(\hat{x}(t)\big) + \lambda_S\, \Omega\big(\nabla_s \hat{x}(t)\big) \Big)\, dt \text{[24]}. \tag{9}$$

where R is measurement covariance, $\Psi(\cdot)$ penalizes violations of invariants such as nonnegative densities and bounded void fraction, and $\Omega(\cdot)$ penalizes nonphysical spatial oscillations introduced by discretization or overfitting. These regularizers are not cosmetic; they are essential to ensure that the learned component remains a correction rather than a surrogate for the physics.

A key question is whether the architecture can generalize across geometries and flow orientations [25]. Many drilling and transport scenarios involve horizontal or highly deviated segments where stratification becomes important. Empirically, flow-regime classification in horizontal two-phase systems can achieve high accuracy with appropriate feature sets and neighborhood-based mod-

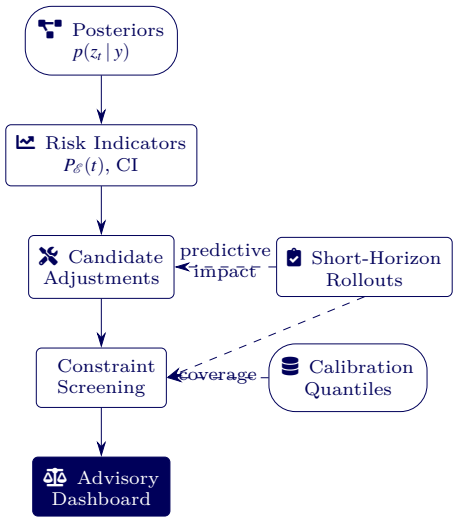

Figure 5. Risk-aware decision support: posterior uncertainty is summarized into interpretable risk indicators and evaluated under a small set of admissible adjustments via short-horizon predictive rollouts; constraint screening and empirical calibration quantiles shape conservative advisories suitable for nonstationary drilling conditions.

els, although performance can vary with parameterization and the train–test mismatch [26]. The proposed architecture leverages this insight differently: rather than directly importing a classifier, it uses regime-aware basis closures and allows the embedding r to shift the model along a physically meaningful manifold. This makes the model less sensitive to the exact regime boundary definitions used in any particular dataset while still capturing the leading-order structural changes associated with orientation and stratification [27].

To enable end-to-end differentiability, the discretized dynamics are integrated with stable, implicit or semi-implicit schemes when stiffness is present, especially in compressible gas transport. Differentiable implicit solvers are feasible when the Jacobian structure is exploited and when regularization prevents ill-conditioning. The digital twin is thus a composable object: the physics core is interpretable and respects conservation, the learned residual is bounded and localized, and the regime embedding provides flexible but structured adaptation [28]. The next section builds on this to perform online inference, where uncertainty quantification and anomaly detection are treated as first-class outputs rather than afterthoughts.

4. Online Inference and Anomaly Detection

A real-time system must continuously ingest streaming surface measurements, update beliefs about latent states and parameters, and issue anomaly indications with controlled false-alarm behavior. This section formulates inference as Bayesian filtering in a constrained nonlinear state-space model, then derives an anomaly score grounded in innovation statistics and mechanistic residuals. The approach emphasizes calibration and robustness under partial observability [29].

Let the augmented state be $z(t) = [x(t)^\top, r(t)^\top, \vartheta(t)^\top]^\top$, where $\vartheta(t)$ includes slowly varying parameters such as effective rheology or friction multipliers. The continuous-time stochastic dynamics can be written as

$$\dot{z}(t) = F_\phi\big(z(t), u(t)\big) + \xi(t), \tag{10}$$

with $\xi(t)$ representing process noise [30]. Measurements satisfy $y(t) = H\big(z(t), u(t)\big) + v(t)$. The filtering objective is the posterior $p(z(t) \mid y_{0:t})$, where $y_{0:t}$ denotes measurements up to time t. Because the model is nonlinear and may be moderately high-dimensional after spatial discretization, approximate inference is required.

A practical choice is a constrained ensemble Kalman filter variant that preserves bounded variables such as void fraction and regime weights through transformations. Let $\tilde{z}$ denote an unconstrained parameterization, with bijections mapping $\tilde{z}$ to z via sigmoid and softplus transforms for bounded components. An ensemble $\{\tilde{z}^{(i)}\}_{i=1}^{M}$ is propagated forward using the differentiable simulator, then updated using a Kalman-like correction based on linearized measurement sensitivity estimated from the ensemble. The update is modified by projection onto constraint sets to avoid violating physical bounds [31]. Although not exact, this approach provides a computationally viable approximation that yields sample-based uncertainty estimates.

When the posterior is highly non-Gaussian, especially during abrupt events, a particle filter can be used on a reduced latent space. The reduction is achieved by learning a low-dimensional latent $l(t)$ that captures the dominant modes of variation in $x(t)$ that are visible from surface sensors, while retaining a mechanistic decoder that reconstructs a physically plausible field [32].

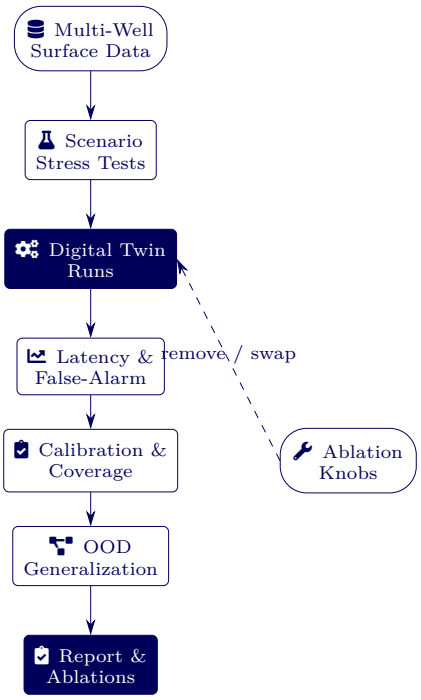

Figure 6. Evaluation protocol emphasizing operational reliability: multi-well surface datasets and controlled stress tests drive repeated digital-twin runs; performance is assessed by detection latency under fixed false-alarm control, probabilistic calibration/coverage diagnostics, and out-of-distribution robustness, complemented by ablations that isolate the contribution of regime awareness, residual learning, and Bayesian inference.

In that case, the inference model becomes

$$\dot{l}(t) = a_\phi\big(l(t), u(t)\big) + \varepsilon(t), \quad x(t) \approx D_\phi\big(l(t), u(t)\big), \tag{11}$$

where D_ϕ is constrained to satisfy conservation in expectation by embedding the decoder inside the physics integrator. This hybrid latent filtering reduces computational cost while maintaining interpretability through the decoder and physics core [33].

Anomaly detection is framed as hypothesis testing on the innovation process. Let $\hat{y}(t \mid t^-)$ be the one-step-ahead predictive mean and $S(t)$ the predictive covariance from the filter. The normalized innovation is

$$\nu(t) = S(t)^{-1/2}\big(y(t) - \hat{y}(t \mid t^-)\big). \tag{12}$$

Under nominal conditions and correct calibration, $\nu(t)$ should be approximately standard normal (in discrete time) after accounting for serial correlation induced by sensor filtering [34]. Deviations indicate either an unmodeled disturbance, a sensor fault, or a physical anomaly such as an influx or loss. A basic anomaly score is the quadratic form

$$\mathscr{A}_I(t) = \nu(t)^\top \nu(t), \tag{13}$$

but this alone is insufficient because it conflates mismodeling and anomalies. The proposed digital twin therefore decomposes residuals into mechanistic channels [35]. Let $e_\tau(t)$ denote the inferred correction to friction, $e_s(t)$ the correction to slip, and $e_q(t)$ an inferred distributed source term needed to reconcile mass balance. These quantities are not directly observed but can be inferred as part of the augmented state. The anomaly score then combines innovation evidence with physically meaningful residual structure: [36]

$$\begin{aligned}\mathscr{A}(t) = {} & \mathbb{E}\big[\mathscr{A}_I(t) \mid y_{0:t}\big] \\ & + \gamma_q\, \mathbb{E}\big[\|e_q(t)\|_1 \mid y_{0:t}\big] \\ & + \gamma_\kappa\, \mathbb{E}\big[\kappa(t) \mid y_{0:t}\big].\end{aligned} \tag{14}$$

where $\kappa(t)$ is a curvature or roughness penalty indicating whether the inferred residuals require spatially oscillatory structure that would be physically implausible. High innovation coupled with a localized, plausible mass source residual supports a physical anomaly hypothesis, whereas high innovation coupled with implausible residual structure suggests sensor faults or boundary inconsistencies.

Change detection is implemented by monitoring the cumulative log-likelihood ratio between a nominal model and an alternative model that allows a change in the source term or in selected parameters. Let $\ell_0(t)$ be the log-likelihood under nominal dynamics and $\ell_1(t)$ under a change-allowed model [37]. A generalized likelihood

Aspect	Purely data-driven detector	Physics-constrained digital twin (⚙)
Structural prior	Minimal; relies on statistical regularities	Encodes conservation laws and wellbore hydraulics explicitly
Uncertainty output	Often point scores or uncalibrated probabilities	Calibrated posteriors over latent states and parameters
Interpretability	Limited feature-based explanations	Mechanistic explanations via residuals and inferred source terms
Generalization	Sensitive to train–test mismatch	Extrapolates using physics; residuals adapt to local conditions
Regime handling	Implicit in training data	Continuous regime embedding influencing closures
Sensor artifacts	Tends to overfit measurement quirks	Explicit sensor dynamics and delays in measurement model
Decision support	Thresholded alarms	Risk metrics and short-horizon probabilistic forecasts

Table 1. Conceptual contrast between surface-only discriminative detectors and the proposed physics-constrained digital twin.

ratio statistic is

$$G(t) = \max_{\tau \in [t-W,t]} \int_{\tau}^{t} \big(\ell_1(\boldsymbol{\sigma}) - \ell_0(\boldsymbol{\sigma})\big)\, d\boldsymbol{\sigma}, \tag{15}$$

where W is a sliding window. An alarm is triggered when $G(t)$ exceeds a threshold chosen to control the average run length under nominal conditions [38]. Because drilling data are nonstationary, the threshold is adaptively adjusted using the filter's own calibration diagnostics, such as the empirical distribution of $\mathscr{A}_I(t)$ during verified nominal intervals.

A practical system must also handle sensor dropouts and asynchronous sampling. The filter therefore supports missing data by skipping updates for absent channels and inflating process noise to reflect increased uncertainty. For delayed measurements, the system uses a fixed-lag smoother over a short horizon, re-integrating the differentiable simulator to incorporate late-arriving evidence without introducing inconsistency. This is computationally feasible because the reduced-order model and the learned residual are designed for fast evaluation [39].

The output of online inference is not merely an alarm. It is a posterior distribution over latent annular states, closure corrections, and potential source terms. This distribution can be interrogated to answer operationally relevant questions: whether an anomaly is likely, where along the well it is most consistent with the data, and how uncertain that localization is [40]. The next section shows how to translate these probabilistic outputs into decision support that respects constraints and avoids overconfident recommendations.

5. Risk-Aware Decision Support

Anomaly detection becomes operationally meaningful only when it is coupled to a decision layer that accounts for uncertainty, constraints, and the cost asymmetry between false negatives and false positives. This section proposes a mapping from the digital twin's posterior outputs to risk metrics and constraint-aware advisories, emphasizing interpretability and conservatism without prescribing procedural actions.

Let $\mathscr{E}$ denote an event class of concern, such as an influx-like anomaly, a loss-like anomaly, or a sensor inconsistency. Define an event probability computed from the posterior over inferred source terms and residual patterns: [41]

$$P_{\mathscr{E}}(t) = \mathbb{P}\big(\mathscr{E} \mid y_{0:t}\big). \tag{16}$$

For an influx-like anomaly, $\mathscr{E}$ can be operationally characterized as posterior mass on positive distributed gas source terms above a tolerance over a contiguous region, together with pressure-consistent transport. Because any single scalar summary can be misleading, the framework provides a vector of risk indicators, such as the posterior mean and credible interval of inferred influx rate, the probability that the inferred source is near

Symbol	Meaning	Typical role
$s \in [0, L]$	Measured depth coordinate along the wellbore	Spatial index for discretization cells
$t \geq 0$	Time	Index for dynamic evolution and filtering
$\alpha(s,t)$	Gas void fraction	Controls mixture density and compressibility
$\rho_m(s,t)$	Mixture density	Appears in mass and momentum balance
$u_m(s,t)$	Mixture velocity	Drives convective transport and pressure losses
$p(s,t)$	Annular pressure	Primary state linked to surface pressure signals
$q_m(s,t)$	Distributed mass source term	Represents influxes, losses, and unmeasured disturbances

Table 2. Representative variables and symbols used in the reduced-order annular multiphase flow model.

Component	Contents	Examples
State $x(t)$	Discretized pressure, velocity, gas fraction fields	Cell-averaged p, u_m, gas mass fraction
Regime embedding $r(t)$	Low-dimensional representation of flow pattern	Weights for basis friction and slip closures
Slow parameters $\vartheta(t)$	Slowly drifting effective properties	Friction multipliers, rheology surrogates
Control inputs $u(t)$	Actuated boundary conditions	Pump rate, choke opening or backpressure
Measurements $y(t)$	Surface-accessible signals	Standpipe pressure, casing pressure, flow-in/out, pit volume rate

Table 3. Key elements of the augmented state-space formulation used in the digital twin observer.

the bit versus higher in the annulus, and the probability that the system is in a high-slip, high-void regime associated with rapid migration.

Decision support is posed as a constrained optimization under partial observability. Let $u(t)$ represent adjustable boundary inputs, and let $c(z,u)$ represent constraints such as pressure limits and equipment bounds. A risk functional can be defined as [42]

$$\mathscr{R}(u;t) = \mathbb{E}\Big[\mathscr{C}\big(z(t),u(t)\big) \;\Big|\; y_{0:t}\Big], \tag{17}$$

where $\mathscr{C}$ penalizes states that violate safety margins or that increase the likelihood of escalation. The advisories are generated by evaluating how candidate adjustments would shift the predicted risk over a short horizon, using the digital twin as a stochastic predictor:

$$\min_{u(\cdot)} \mathbb{E}\Big[\int_t^{t+T_h} \mathscr{C}\big(z(\sigma),u(\sigma)\big)\, d\sigma \;\Big|\; y_{0:t}\Big] \quad \text{subject to} \quad c\big(z(\sigma),u(\sigma)\big) \leq 0. \tag{18}$$

In practice, rather than solving a full stochastic control problem online, the system evaluates a small set of admissible adjustments and reports the predicted effect on risk metrics, along with uncertainty bounds. This keeps the layer interpretable and avoids the impression of an autonomous controller [43]. The output is framed as probabilistic guidance: for example, whether the posterior probability of an influx-like event would decrease under a more conservative boundary condition, and how that change compares to uncertainty.

A critical issue is avoiding overconfidence. Even a

Aspect	Physics core f_{phy}	Learned residual Δ_ϕ
Mass conservation	Enforces balance of mixture and gas mass	Does not create or destroy mass directly
Momentum balance	Governs inertial, pressure, and gravitational forces	Adjusts effective wall shear contribution
Closures	Provides nominal friction and drift-flux parameters	Adds bounded corrections to closure values
Regime effects	Basis closures parameterized by embedding r	Learns dynamics of $r(t)$ and smooth transitions
Sensor modeling	Includes nominal sensor filters and delays	Compensates for unmodeled sensor idiosyncrasies
Distributed sources	Contains baseline formation influx/loss models	Captures residual source terms consistent with data

Table 4. Division of responsibilities between mechanistic model components and learned closure residuals.

Inference method	Strengths	Limitations
Constrained EnKF	Ensemble-based uncertainty, scalable to many states	Approximate Gaussian assumptions; may struggle with severe nonlinearity
Particle filter in latent space	Handles non-Gaussian posteriors in reduced dimension	Requires informative latent representation and more samples
Deterministic simulator + thresholds	Simple implementation, low computational burden	No explicit uncertainty; brittle under distribution shift
Fixed-lag hybrid smoother	Incorporates delayed data and refines recent states	Additional computation and buffering, limited smoothing horizon

Table 5. Online inference strategies considered for real-time estimation of latent wellbore states.

calibrated filter can become miscalibrated under severe out-of-distribution conditions. To mitigate this, the decision layer uses conformal-style calibration on the anomaly score and on key posterior summaries [44]. Given historical nominal segments, the system estimates quantiles of $\mathscr{A}(t)$ and of selected residual norms; it then reports whether the current values exceed calibrated thresholds at, for example, 95% nominal coverage. This does not prove correctness, but it enforces a disciplined representation of uncertainty and helps operators understand when the model is extrapolating.

Interpretability is enhanced by generating mechanistic explanations tied to the inferred residual structure. If the posterior places significant mass on a localized positive gas source term with modest friction correction, the explanation is framed as a mass-balance-consistent anomaly [45]. If instead the posterior requires widespread friction increases without coherent mass sources, the explanation emphasizes likely rheology drift or cuttings-related effects. When the posterior indicates a sensor inconsistency, the system highlights which measurement channels drive the innovation and how sensitive the inference is to their inclusion. These explanations are derived from the model structure rather than from ad hoc feature attribution methods, which are often fragile in time-dependent systems.

The decision support layer thus treats the digital twin as a probabilistic lens: it converts surface signals into physically constrained hypotheses and quantifies uncertainty [46]. The next section describes how to evaluate such a system rigorously, with metrics that reflect latency, calibration, and generalization rather than only classification accuracy.

6. Evaluation Framework and Implementation Considerations

Evaluating a physics-constrained digital twin differs from evaluating a purely discriminative classifier because the outputs include state posteriors, residual decompositions, and risk metrics. Moreover, ground truth for downhole states is often unavailable, so evaluation must combine partial labels, synthetic stress tests, and consistency checks [47]. This section proposes an evaluation framework and discusses implementation considerations

Hypothesized cause	Innovation behaviour	Residual structure in the twin
Influx-like anomaly	Persistent positive pressure/flow mismatch	Localized positive mass source term with plausible migration pattern
Loss-like anomaly	Drop in pressure not explained by controls	Localized negative mass source, consistent with outflow to formation
Rheology drift / cuttings loading	Gradual pressure increase and lagged response	Widespread friction correction without strong localized sources
Sensor fault	Large innovation concentrated in few channels	Inconsistent residuals; inferred states diverge from sensor pattern
Choke or boundary mis-modeling	Mismatch near outlet conditions	Residuals concentrated at boundary cells and associated parameters

Table 6. Qualitative connection between anomaly hypotheses, innovation statistics, and inferred residual patterns.

that influence real-time viability.

A primary metric is detection latency under controlled anomaly injections. When synthetic scenarios are available, an influx-like source term can be injected into the physics core while generating surface measurements through the same simulator plus realistic sensor noise and filtering. The digital twin is then run as if on real data, and the time-to-detection distribution is computed [48]. Latency must be reported jointly with false-alarm rate because aggressive thresholds can reduce latency at the cost of nuisance alarms. The framework therefore fixes a nominal false-alarm rate and compares latency across methods. When synthetic scenarios are not trusted due to model mismatch, a hybrid approach can be used: real nominal surface time series are perturbed by physically plausible residual patterns learned from data, and the system's response is measured [49]. This preserves sensor characteristics while still enabling controlled anomaly timing.

Calibration is evaluated via probability integral transform diagnostics on predicted measurement distributions and via coverage tests on posterior credible intervals for key summaries. For example, if the model predicts a 90% credible interval for surface pressure over a horizon, the empirical frequency with which observed pressure lies in that interval should be close to 90% under nominal conditions. Miscalibration is expected under distribution shift; the evaluation should therefore include stratified analysis across operating envelopes, such as different pump rates, mud weights, and choke regimes [50]. Reporting only global calibration can hide systematic miscalibration in rare but critical regimes.

A second family of metrics concerns physical consistency. Because the digital twin outputs inferred residuals such as effective source terms and friction corrections, one can test whether these residuals remain sparse and plausible under nominal conditions [51]. Excessive reliance on residuals indicates that the learned component is compensating for systematic modeling errors, potentially undermining interpretability. A useful diagnostic is the fraction of time the posterior mass of e_q exceeds a small threshold under nominal segments; this should be low and stable across wells if the model is robust. Another diagnostic is whether inferred regime embeddings remain within expected bounds and transition smoothly except when evidence supports abrupt changes.

Generalization is tested across geometry and orientation by training on a subset of wells or loop configurations and evaluating on others with different hydraulic diameters, inclinations, and sensor characteristics [52]. The hybrid architecture is expected to generalize better than a purely data-driven detector because conservation structure is invariant. However, closure mismatch can still be significant when fluids or cuttings load change. The evaluation should therefore include out-of-distribution tests such as altered rheology, delayed sensors, and unmodeled choke nonlinearity [53]. Performance degradation should be characterized not only by detection accuracy but by increased uncertainty and by the system's ability to flag that it is extrapolating, for instance through increased innovation variance and wider posteriors.

Implementation must respect real-time constraints. The differentiable simulator should run faster than wall-clock time at the chosen discretization. This motivates adaptive spatial resolution: finer discretization near regions of high compressibility or expected regime transition, coarser elsewhere [54]. It also motivates caching

Indicator	Description	Typical use in operations
$P_{\text{influx}}(t)$	Posterior probability of influx-like event class	Screening for potential kicks and escalation risk
Expected influx rate	Posterior mean of inferred positive source term	Assessing severity and potential growth of anomaly
Influx depth probability	Distribution of source location along s	Prioritizing attention near bit, shoe, or upper annulus
High-slip regime probability	Chance of being in gas-dominated transport regime	Anticipating rapid gas migration and pressure response
Pressure margin	Distance to upper and lower pressure constraints	Evaluating safety margins under candidate control actions
Composite anomaly score $\mathscr{A}(t)$	Fusion of innovation and residual metrics	Triggering alarms under controlled false-alarm targets

Table 7. Representative risk indicators derived from the posterior distribution produced by the digital twin.

Jacobian structure for implicit steps and using ensemble sizes that balance uncertainty representation with computational cost. In many cases, an ensemble size M in the tens can be sufficient for stable filtering if the model is well-regularized, whereas particle filtering may require more samples unless the latent dimension is aggressively reduced.

Sensor pre-processing is another crucial factor [55]. The system must treat measurements as the output of a sensor dynamics model, not as direct samples of the physical variables. Low-pass filtering, rate limiting, and quantization can introduce phase lags that shift anomaly signatures in time, biasing latency estimates. The framework therefore includes identification of sensor filters from nominal data by fitting simple linear time-invariant models, then incorporating them into $h(\cdot)$ so that the filter operates on physical predictions rather than on raw data streams. This alignment reduces the temptation for the learned residual to compensate for sensor artifacts [56].

Finally, ablation studies are essential to verify that each architectural element contributes to robustness rather than merely increasing capacity. Ablations can remove the regime embedding, remove closure residual learning, or remove probabilistic inference in favor of deterministic simulation with thresholding. The expectation is that removing probabilistic inference will reduce calibration and robustness under partial observability, while removing physics constraints will increase false positives under distribution shift [57]. These claims must be tested empirically, but the framework is designed to make such tests meaningful by reporting calibration, residual plausibility, and stability alongside detection metrics.

The evaluation framework thus aligns with the paper's thesis: a wellbore anomaly detector should be judged by its ability to provide trustworthy probabilistic physical inference from surface signals, not only by accuracy on a curated dataset. The concluding section summarizes the contributions and outlines the main limitations and future directions implied by the formulation.

7. Conclusion

This paper presented a physics-constrained, uncertainty-aware digital-twin framework for real-time wellbore anomaly detection using primarily surface measurements [58]. The core idea is to treat detection as probabilistic state estimation in a structured dynamical system rather than as a standalone classification task. A reduced-order annular multiphase model provides conservation structure and interpretability, while a learned closure residual corrects only selected mismatches under hard physical constraints. A latent regime embedding enables soft, physically meaningful transitions without requiring brittle discrete regime labels [59]. Online inference is performed through approximate Bayesian filtering with constraint-preserving transforms, producing calibrated posteriors over latent states, closure corrections, and inferred source terms. Anomaly detection is derived from innovation statistics augmented by mechanistic residual decompositions, enabling differentiation between physical anomalies, systematic modeling errors, and sensor inconsistencies. A risk-aware decision-support layer maps posterior outputs to constraint-aware advisories using short-horizon stochastic prediction while explicitly accounting for uncertainty.

The paper also proposed an evaluation framework emphasizing detection latency under fixed false-alarm control, calibration and coverage diagnostics, residual plausibility under nominal conditions, and out-of-distribution

Metric	What it measures	Notes for interpretation
Detection latency	Time from anomaly onset to alarm	Reported jointly with fixed false-alarm rate
False-alarm rate	Frequency of spurious alarms in nominal data	Evaluated across operating envelopes and wells
Calibration / coverage	Agreement between predicted and empirical probabilities	Uses prediction intervals and innovation statistics
Residual sparsity	How often large source residuals appear when nominal	High values suggest overfitting or model structural errors
Regime consistency	Plausibility and smoothness of embedding trajectories	Checks for unrealistic regime hopping without evidence
OOD robustness	Performance under geometry, fluid, or sensor shifts	Includes stress tests with altered closures and delays
Computational load	Cost relative to real-time requirements	Considers ensemble size, discretization, and solver choice

Table 8. Evaluation metrics for assessing reliability and robustness of the anomaly detection digital twin.

generalization across geometries, orientations, and sensor characteristics [60]. The formulation highlights that reliability in this domain depends as much on calibrated uncertainty and physical consistency as on nominal predictive accuracy.

Limitations follow directly from the assumptions made for tractability: reduced-order models can omit higher-dimensional effects, closure learning can still fail under extreme distribution shift, and partial observability can prevent unique localization without additional sensors. These limitations motivate future work on adaptive discretization, richer yet still constrained closure manifolds, and principled integration of intermittent downhole measurements when available. Nonetheless, the proposed digital twin provides a coherent mathematical basis for translating surface evidence into probabilistic, physically grounded anomaly assessments suitable for real-time operational contexts [61].

References

[1] I. J. Laurenzi, J. A. Bergerson, and K. Motazedi, "Life cycle greenhouse gas emissions and freshwater consumption associated with bakken tight oil.," Proceedings of the National Academy of Sciences of the United States of America, vol. 113, pp. 201607475–E7680, 11 2016.

[2] "Contaminant plumes containment and remediation focus area. technology summary," 6 1995.

[3] C. Obi, Y. Falola, K. Manikonda, A. Hasan, I. Hassan, and M. Rahman, "A machine learning approach for gas kick identification," SPE Drilling & Completion, vol. 38, no. 04, pp. 663–681, 2023.

[4] O. T. Gudmestad and K. Traa, "Sustainable use and production of energy in the 21st century," International Journal of Energy Production and Management, vol. 1, pp. 1–15, 6 2015.

[5] A. S. A. Sheidi, H. A. R. A. Balushi, Z. A. A. Rawahi, A. S. A. Harrasi, D. Mansur, M. M. A. Farsi, H. S. A. Rubaiey, N. A. A. Harrasi, M. K. Choudhary, and C. Orta, "Step change in controlling the gas-cap in highly depleted and fractured formation," in ADIPEC, SPE, 10 2022.

[6] N. Carrejo, O. R. Espinoza, H. Wibowo, and S. L. Gaudette, "Developing a new high-strength, lightweight material using nano-coated smart materials for oilfield applications," in OTC Brasil, OTC, 10 2015.

[7] C. Carpenter, "Integrated work flow aids data digitization, management for offshore drilling," Journal of Petroleum Technology, vol. 73, pp. 49–50, 10 2021.

[8] N. Carrejo, O. R. Espinoza, H. Wibowo, and S. L. Gaudette, "Developing an innovative nano-coated, smart material to optimize efficiency of oilfield completion applications," in SPE Annual Technical Conference and Exhibition, SPE, 10 2014.

[9] L. Liu, D. Zhan, D. Spencer, and D. Molyneux, "Pack ice forces on floating offshore oil and gas exploration systems," in SNAME 9th International Conference and Exhibition on Performance of Ships and Structures in Ice, SNAME, 9 2010.

[10] Y. Peysson and B. Herzhaft, "Lubrication process at the wall in foam flow application to pressure drop estimation while drilling ubd wells," Journal of Canadian Petroleum Technology, vol. 47, pp. 26–30, 6 2008.

[11] P. Cavanagh, D. Stiles, S. Lemp, and K. Faurschou, "New cementing technology eliminates remediation, reduces risk and lowers well costs in the deep foothills of western alberta," Journal of Canadian Petroleum Technology, vol. 43, pp. 45–51, 6 2004.

[12] C. John, G. Maciasz, and B. Harder, "Gulf coast geopressured-geothermal program summary report compilation. volume 4: Bibliography (annotated only for all major reports)," 6 1998.

[13] H. V. Vu and L. Cao, "On the appraisal and development of st-x field: uncertainties and challenges," Science and Technology Development Journal, vol. 17, pp. 110–116, 9 2014.

[14] F. Fleyfel, C. Silva, G. Okoh, O. Ilesanmi, A. Rivas-Cardona, E. Marotta, and J. Fayemi, "Multiphase cfd cool-down behaviors of an evdt and manifold systems," in Offshore Technology Conference, OTC, 5 2013.

[15] K. Manikonda, A. R. Hasan, C. E. Obi, R. Islam, A. K. Sleiti, M. W. Abdelrazeq, and M. A. Rahman, "Application of machine learning classification algorithms for two-phase gas-liquid flow regime identification," in Abu Dhabi International Petroleum Exhibition and Conference, p. D041S121R004, SPE, 2021.

[16] E. Ahrens and F. Hansen, "Large-scale dynamic compaction demonstration using wipp salt: Fielding and preliminary results," 10 1995.

[17] M. Okot, M. Campos, G. Muñoz, A. Alalsayednassir, M. Weber, and Z. Muneer, "Utilization of an innovative tool to improve hole cleaning efficiency in extended reach wells in saudi arabia," in SPE Kuwait Oil and Gas Show and Conference, SPE, 10 2015.

[18] W. Zhu and X. Zheng, Study on the Rheological Properties of Ultra-High Temperature CGA Drilling Fluids. IOS Press, 12 2021.

[19] P. Konstantin, V. Sergey, and V. Olga, "Specifics of development, infrastructure construction and production of oil-gas-condensate fields. integrated model application experience," in SPE Russian Petroleum Technology Conference, SPE, 10 2017.

[20] "Geothermal energy r&d program annual progress report for fiscal year 1992," 7 1993.

[21] A. Kamel, "A technical review of radial jet drilling," Journal of Petroleum and Gas Engineering, vol. 8, pp. 79–89, 10 2017.

[22] C. Winter and A. Edgington, "Computer analysis of gas field deliverability and development economics," Journal of Canadian Petroleum Technology, vol. 3, pp. 180–186, 12 1964.

[23] T. J. Hammons, Geothermal Power Generation: Global Perspectives, Technology, Direct Uses, Plants, Drilling and Sustainability Worldwide. In-Tech, 6 2011.

[24] "Equipment and services for worldwide applications," 1 1985.

[25] C. Wei and Y. Chen, "Data assimilation-based real-time estimation of downhole gas influx rate and void fraction distribution in a drilling riser," in Volume 10: Petroleum Technology, American Society of Mechanical Engineers, 6 2022.

[26] K. Manikonda, R. Islam, C. E. Obi, A. R. Hasan, A. K. Sleiti, M. W. Abdelrazeq, I. G. Hassan, and M. A. Rahman, "Horizontal two-phase flow regime identification with machine learning classification models," in International Petroleum Technology Conference, p. D011S021R002, IPTC, 2022.

[27] K. D. Newell and T. Birdie, "Geothermal anomalies on the eastern flank of the cherokee basin, southeastern kansas, usa," Midcontinent Geoscience, vol. 2, pp. 54–85, 12 2021.

[28] "Environmental impact assessment for steeply dipping coal beds: North knobs site," 11 1978.

[29] C. D. Gentillon, "Ngnp data management and analysis system analysis and web delivery capabilities," 9 2011.

[30] G. Colodette, C. G. Pereira, C. A. M. Siqueira, G. S. Ribeiro, R. Rodrigues, J. S. de Matos, and M. P. Ribeiro, "The new deepwater oil and gas province in brazil: Flow assurance and artificial lift: Innovations for jubarte heavy oil," in Offshore Technology Conference, OTC, 4 2007.

[31] A. T. Bozdana, N. Al-Kharkhi, and K. Al-Kharkhi, "Comparative experimental and numerical investigation on electrical discharge drilling of aisi 304 using circular and elliptical electrodes," Strojniški vestnik - Journal of Mechanical Engineering, 4 2018.

[32] I. Ortiz, R. Anthony, J. Gabrielson, and R. Glickert, "Low nosub x turbine power generation utilizing low btu gob gas. final report, june–august 1995," 8 1995.

[33] G. Zhao, S. Tang, Z. Liang, and J. Li, "Dynamic stability of a stepped drillstring conveying drilling fluid," Journal of Theoretical and Applied Mechanics, vol. 55, pp. 1409–1422, 10 2017.

[34] "Western gas sands project status report," 4 1978.

[35] E. Gilbertson, F. S. Hover, and E. Colina, "Failure mode and sensitivity analysis of gas lift valves," in

29th International Conference on Ocean, Offshore and Arctic Engineering: Volume 2, pp. 305–314, ASMEDC, 1 2010.

[36] I. Gunawan and R. Rubiandini, "Determining cutting transport parameter in a horizontal coiled tubing underbalanced drilling operation," in SPE Asia Pacific Oil and Gas Conference and Exhibition, SPE, 10 2002.

[37] M. M. Al-Khudiri, M. A. A. Shehry, and J. Curtis, "Data architecture of real-time drilling and completions information at one company," in SPE Russian Oil and Gas Technical Conference and Exhibition, SPE, 10 2008.

[38] O. Baris, L. F. Ayala, and W. W. Robert, "Numerical modeling of foam drilling hydraulics," The Journal of Engineering Research [TJER], vol. 4, pp. 103–119, 12 2007.

[39] M. S. Turbakov and leksandr Shcherbakov, "Determination of enhanced oil recovery candidate fields in the volga-ural oil and gas region territory," Energies, vol. 8, pp. 11153–11166, 10 2015.

[40] S. Blackburn, R. Sanders, C. Boyer, E. Lasseter, J. Stevenson, and R. Mills, "Demonstration of the enrichment of medium quality gas from gob wells through interactive well operating practices. final report, june–december, 1995," 12 1995.

[41] N. Lior, "Exergy, energy, and gas flow analysis of hydrofractured shale gas extraction," Journal of Energy Resources Technology, vol. 138, pp. 061601–, 2 2016.

[42] H. S. Littell, J. W. Jessup, W. Schoppa, M. Seay, and T. Coulon, "Perdido startup: Flow assurance and subsea artificial lift performance," in Offshore Technology Conference, OTC, 5 2011.

[43] "Feasibility study of a hybrid erosion drilling concept," 6 1977.

[44] V. Naik, H. Bahman, S. M. Al-Haddad, and F. Ali, "Production optimization from a short lateral horizontal well in a braided fluvial deposition system: A case study from greater burgan field, kuwait.," in SPE Kuwait Oil & Gas Show and Conference, SPE, 10 2017.

[45] J. Burger, D. Gupta, P. Jacobs, and J. Shillinglaw, "Overview on hydrate coring, handling and analysis," 6 2003.

[46] K. Dollens, K. Harpole, E. Durrett, and J. Bles, "Design and implementation of a cosub 2 flood utilizing advanced reservoir characterization and horizontal injection wells in a shallow shelf carbonate approaching waterflood depletion. annual report, july 1, 1996–june 30, 1997," 12 1997.

[47] Q. Ashraf, A. Khalid, and S. A. Hussain, "Electromagnetic measurement while drilling system enabled the operator to reach beyond the limits in a multiphase foam drilling medium," in Offshore Technology Conference Asia, OTC, 3 2022.

[48] J. A. Bamberger and M. S. Greenwood, "Evaluation of ultrasonic methods for in-situ real-time characterization of drilling mud," in Volume 2: Fora, pp. 499–504, ASMEDC, 1 2005.

[49] J. C. Almeida, M. Rangel, G. Rey, M. Pacione, C. López, and A. Valdivieso, "Well of the future: A new approach to real-time wellbore stability monitoring in the colombian foothills," SPE/IADC Drilling Conference and Exhibition, 3 2015.

[50] B. Huang and Y. Wang, "Roof weakening of hydraulic fracturing for control of hanging roof in the face end of high gassy coal longwall mining: a case study," Archives of Mining Sciences, vol. 61, pp. 601–615, 9 2016.

[51] M. Golbabaei-Asl, A. Povitsky, and L. Ring, "Cfd modeling of fast transient processes in drilling fluid," in Volume 7A: Fluids Engineering Systems and Technologies, American Society of Mechanical Engineers, 11 2015.

[52] I. Silvestrov, E. Hemyari, A. Bakulin, Y. Luo, A. Aldawood, F. Poletto, Y. Liu, Y. Du, A. Egorov, and P. Golikov, "Processing of seismic-while-drilling data from the drillcam system acquired with wireless geophones, top-drive, and downhole vibrations sensors," in SPE Middle East Oil & Gas Show and Conference, SPE, 12 2021.

[53] A. Layne and A. Yost, "Development of advanced drilling, completion, and stimulation systems for minimum formation damage and improved efficiency: A program overview," in SPE Formation Damage Control Symposium, SPE, 2 1994.

[54] E. D. Gomez, M. Chavarria, J. C. Beltran, C. P. M. Lupo, H. Duno, and J. Casaos, "Successful use of managed pressure drilling (mpd) in low pressure, high pressure, and deeper reservoirs in mexico south," in SPE/IADC Managed Pressure Drilling and Underbalanced Operations Conference and Exhibition, SPE, 3 2012.

[55] R. Harkouss, "Pipeline modelling for the lebanese offshore: Cases in the oil and gas industry," JORDANIAN JOURNAL OF ENGINEERING AND CHEMICAL INDUSTRIES (JJECI), vol. 5, pp. 59–70, 8 2022.

[56] Y. Lu, Z. Zhou, Z. Ge, X. Zhang, and Q. Li, "Research on and design of a self-propelled nozzle for the tree-type drilling technique in underground coal mines," Energies, vol. 8, pp. 14260–14271, 12 2015.

[57] V. K. Y. Kovalenko, Triaxial loading system as a tool for solving geotechnical problems of oil and gas production, pp. 317–326. CRC Press, 8 2012.

[58] "United states geothermal technology: Equipment and services for worldwide applications," 5 1995.

[59] G. Thoma, J. A. Veil, F. Limp, J. Cothren, B. E. Gorham, M. Williamson, P. Smith, and B. Sullivan, "Probabilistic risk based decision support for oil and gas exploration and production facilities in sensitive ecosystems," 5 2009.

[60] M. W. Massey, "Marine well containment company progress," in Offshore Technology Conference, OTC, 4 2012.

[61] G. Subbuswamy and X. Li, "Numerical study of film cooling enhancement in gas turbine combustor liner," in Volume 10: Heat Transfer, Fluid Flows, and Thermal Systems, Parts A, B, and C, pp. 1237–1247, ASMEDC, 1 2008.